PCCP

PAPER

Cite this: *Phys. Chem. Chem. Phys.*, 2019, **21**, 22930

Beyond molecular nitrogen: revelation of two ambient-pressure metastable single- and double-bonded nitrogen allotropes built from three-membered rings†

Sergey V. Bondarchuk

Received 1st August 2019,
Accepted 24th September 2019

DOI: 10.1039/c9cp04288a

rsc.li/pccp

In this study, we present a crystal structure prediction and characterization for two novel single- and double-bonded nitrogen allotropes (denoted as CubN and DobN) bearing three-membered nitrogen cycles. These materials are ambient-pressure metastable robust solids with strong cohesive energies. Due to the presence of strained nitrogen cycles, these allotropes are high-lying phases, which retain high energy densities at least up to 200 GPa, when CubN becomes lower in energy than ζ-N_2. The studied allotropes are indirect wide-bandgap semiconductors. A detailed spectral characterization of these materials is also presented herein. Due to their extremely high heats of formation and crystal densities, CubN and DobN demonstrate excellent detonation properties that are comparable to those of previously reported phases (cg-N and TrigN). Propulsive properties (including specific impulse and characteristic velocity) of CubN and DobN as solid monopropellants were also estimated. Thus, if synthesized, the present nitrogen allotropes will have great potential for practical applications and achieving fundamental knowledge about nitrogen as a chemical element.

Introduction

The development of chemical methods for molecular nitrogen fixation in the form of ammonia brought two Nobel Prizes in chemistry for Fritz Haber and Carl Bosch in 1918 and 1931, respectively. The fundamental importance of these methods is due to their ability to transform the most abundant inert atmospheric gas into an easily functionalizable inorganic substance, which can be used as a building-block for a great variety of compounds (fertilizers, energetic compounds, synthons, *etc.*). Recently, the Haber–Bosch process has been significantly improved, allowing nitrogen fixation under near ambient conditions using transition metal complexes[1] or metal-free compounds.[2] The ability of dinitrogen to bind with transition metals was applied to electrochemical activation at the Ir/YSZ interface, where YSZ – yttria-stabilized zirconia.[3] Moreover, a promising low-temperature N_2 dissociation catalyst, namely, Au(111) surface doped with Mo atoms, was recently predicted.[4] In addition, a possible route towards dinitrogen reactivity *via* its excited triplet $A^3\Sigma_u^+$ state was proposed.[5]

The difficulty with nitrogen fixation lies in the inert nature of the nitrogen molecule, and a huge energy stimulus (945 kJ mol^{-1}) is required to break the triple N≡N bond.[6] This is the reason why compounds bearing the N=N and N–N bonds have high positive enthalpies of formation. As a result, to the best of our knowledge, only three allotropes of nitrogen, other than the molecular crystalline form of N_2, are known experimentally. The first is the so-called cubic *gauche* (cg-N) allotrope, which was detected *via* diamond anvil cell experiments by Eremets *et al.*[7] Note that this form of nitrogen was much earlier predicted to be the lowest-energy single-bonded allotrope. Thus, McMahan *et al.*[8,9] predicted several possible nitrogen allotropes using density functional theory calculations. The second experimentally known allotrope is the layered *Pba*2 phase, which has been found to be stable under 120–180 GPa.[10] Again, this structure was predicted earlier using an evolutionary algorithm for crystal structure search.[11] Finally, the third structure is a molecular N_8 form of nitrogen, which has recently been observed under 40 GPa,[12] and its anionic form N_8^- has also been obtained in a carbon nanotube.[13]

It is interesting that N_8 was spontaneously predicted earlier when calculating the N_4 tetramer.[14] Metadynamics calculations suggest N_8 (and another predicted allotrope N_6[15]) to be thermally metastable at near ambient conditions.[16] Experiment revealed,

Department of Chemistry and Nanomaterials Science, Bogdan Khmelnitsky Cherkasy National University, blvd. Shevchenko 81, 18031 Cherkasy, Ukraine. E-mail: bondchem@cdu.edu.ua

† Electronic supplementary information (ESI) available: Crystal packing, Brillouin zone integration paths, optical properties, nature of electronic bands, graphical and numerical data on vibrational spectra, nuclear magnetic resonance and thermodynamic data, coefficients of the NASA polynomials. See DOI: 10.1039/c9cp04288a

however, that upon pressure release, N_8 remains observable only at 3 GPa.[12] Furthermore, various covalently-bound forms of nitrogen were also predicted using different techniques, but all were higher in energy than the cg-N allotrope. A short review of the predicted nitrogen phases (including molecular crystals) along with space groups and the corresponding references are presented in our recent papers.[17,18]

The nitrogen behavior at high-pressure is rather unexpected. Thus, being compressed together with hydrogen, it forms stable crystalline van der Waals compounds of the following composition: $(N_2)_6(H_2)_7$ and $N_2(H_2)_2$.[19] Such high-pressure chemistry of nitrogen is very important outside the Earth's atmosphere where pressure often reaches tens or even hundreds of gigapascals. For example, it was found that the cg-N allotrope and its ''chemical twin'' (TrigN) become lower in energy than the α-N_2 phase at 53 and 66 GPa, respectively.[17]

Another very important field of research is the potential application of single-bonded nitrogen allotropes as high-energy-density materials (HEDM).[20] Indeed, the relative amount of energy enclosed in the cg-N and TrigN is huge and equals 10.22 and 11.01 kJ g^{-1}, respectively.[17] This is more than five times higher than that of the most powerful non-nuclear weapons.[21] To satisfy all the required criteria for a potential HEDM, the structure must be at least dynamically and mechanically stable at ambient pressure. Recently, a promising allotrope t-N of the tetragonal crystal system (the $P4_1/a$ space group) was predicted and a potential synthetic route *via* He–N compounds was offered.[18] Our present calculations, however, revealed that t-N behaves very similarly to the TrigN allotrope under pressure.[17] Thus, in the pressure range 0–140 GPa, it never appears to be more stable than the cg-N allotrope.

Herein, we have tried to find new dynamically and mechanically stable nitrogen allotropes bearing three-membered nitrogen cycles. Such strained cycles are strongly energetic structural motifs; hence, the corresponding nitrogen allotropes are expected to be more efficient HEDMs as compared to simple single-bonded nitrogen phases. We have not used any structure predictors and all input crystal structures for cell relaxation were constructed manually.

Computational details

In this work, we performed Density Functional Theory (DFT) calculations within the generalized gradient (GGA) and local density (LDA) approximations. All the equilibrium geometries were calculated and the total energies were estimated using norm-conserving (NC)[22] pseudopotentials based on the Perdew–Burke–Ernzerhof (PBE) functional.[23] Meanwhile, for the Quantum Chemistry of Atoms in Molecules (QTAIM) analysis, the projector augmented wave (PAW)[24] method was utilized. For the above-mentioned calculations, the electronic wave functions were expanded in a plane wave basis set with an energy cutoff of 1200 eV (88.2 Ry), which was applied along with the finite basis set correction procedure. The sampling of the Brillouin zones was performed using *k*-point grids generated by the Monkhorst–Pack method. Direct spacing between *k*-points was specified to 0.08 $Å^{-1}$ for all the cell relaxations and 0.05 $Å^{-1}$ for the electronic, spectral, thermodynamic and mechanical properties calculations. Convergence criteria for the total energy were set to 5×10^{-6} eV $atom^{-1}$ in the SCF calculations and 1×10^{-6} eV $atom^{-1}$ during the fixed geometry calculations.

Heats of formation calculations were performed with a set of pure GGA (PBE), LDA (CA-PZ[25]) and hybrid (B3LYP,[26] PBE0[27] and HSE06[28]) functionals. Dispersion effects were taken into account by means of the Grimme form of the damped C_6 term in the GGA[29] and by means of the Ortmann–Bechsted–Schmidt method[30] in LDA. For the GGA and LDA calculations, the electronic wave functions were obtained by the density-mixing scheme,[31] while for the hybrid functionals, the preconditioned conjugate gradients method was applied.[32] The Broyden, Fletcher, Goldfarb and Shannon (BFGS) method[33] for geometry optimization was applied entirely. Time-dependent DFT (TD-DFT) calculations were performed using the Tamm-Dankoff approximation.[34]

All the calculations with norm-conserving pseudopotentials were carried out using the Cambridge Serial Total Energy Package (CASTEP) code[35] implemented in the Materials Studio 7.0 program suite.[36] The calculations with the PAW approach were performed by means of the Quantum Espresso 5.3.0 package.[37] Molecular visualizations were carried out using the Virtual Nano-Lab 2016.3 program.[38] Topological analysis of crystals was performed using the Critic2 program[39] and the Bader charges were obtained by means of the Bader code.[40]

Results and discussion

Structural features and stability criteria

The discussed CubN and DobN nitrogen allotropes are in the cubic (space group $P2_13$) and trigonal (space group $R3$) crystal systems, respectively. The latter can be presented in two ways using the rhombohedral-centered hexagonal (HEX) or primitive-centered rhombohedral (RHL_2) (for $\alpha > 90^\circ$) lattice. Most of the discussions will be concerned with the RHL_2 lattice. The zero-pressure optimized lattice parameters along with the cohesive energies (E_{coh}) are listed in Table 1 and the corresponding Wyckoff positions (WP) for the symmetry-unique atoms along with their fractional coordinates and Bader charges (q) are gathered in Table 2. As one can see in Table 1, CubN and DobN both have strong cohesive energies close to those of the known allotropes; thus, they can be characterized as robust solids. However, they are slightly less dense materials.

Crystal structures of the studied allotropes are illustrated in Fig. 1 and the crystal packing of DobN is presented in Fig. S1 in the ESI.† The unique structure of the CubN and DobN allotropes

Table 1 The optimized lattice parameters and cohesive energies

Phase	a (Å)	α (°)	Å^3/atom	E_{coh} (eV)
cg-N	3.839		7.03	6.64
TrigN	4.548	98.39	7.46	6.52
CubN	5.174		8.44	6.24
DobN	5.181	95.60	11.41	6.64

Table 2 Fractional coordinates, Wyckoff positions and Bader charges

Allotrope	Atom	WP	x	y	z	q (e)
CubN	N1	12b	0.120	0.262	0.366	0.004
	N2	4a	0.106	0.394	0.606	−0.012
DobN	N1	3b	0.989	0.620	0.977	0.029
	N2	3b	0.442	0.715	0.920	−0.013
	N3	3b	0.673	0.434	0.580	−0.004
	N4	3b	0.215	0.733	0.038	−0.012

Table 3 The QTAIM parameters (a.u.) at several bond and ring CPs

Allotrope	Topology	$\rho(r)$	$\nabla^2\rho(r)$	$G(r)$
CubN	N1–N1	0.224931	−0.044767	0.638491
	N1–N2	0.313862	−0.525502	0.825807
	Cycle	0.157201	0.553587	0.570701
DobN	N1–N2	0.273602	−0.331477	0.735906
	N2–N3	0.337969	−0.683627	0.875655
	N3–N3	0.231002	−0.037264	0.657133
	N1–N4	0.442023	−1.261338	1.108917
	N2–N4	0.365442	−0.808761	0.939334
	Cycle	0.162279	0.538138	0.580415

includes three-membered nitrogen cycles (Fig. 1). These have the bonding pattern as in triaziridine (H_3N_3), a theoretically and experimentally known molecule.[41–43] Due to the high enthalpy of formation and extremely stable products formed, H_3N_3 and its nitro derivatives were considered as potential high-energy-density materials (HEDM).[44,45] The N–N bond lengths in the cycles are slightly higher (Fig. 1) than in bare *cis*- and *trans*-triaziridine (1.47 Å at the G3 level of theory).[44]

Structurally, the CubN allotrope can be imagined as a tertiary amino group connected with three three-membered nitrogen cycles. In the case of DobN, a tertiary amino group is bound to one such cycle and two double N=N bonds (Fig. 1e). The 2D topology of the studied allotropes is presented for clarity in Fig. 1g and h. The lengths of these bonds (1.269 Å) are typical for the N=N bond length in organic compounds.[46] It follows from the Bader charges (Table 2) that there is a very weak polarization of the N–N bonds in both allotropes. Meanwhile, taking into account the negative values of $\nabla^2\rho(r)$, all the N–N bonds are covalent (Table 3).

It is interesting to estimate ring strain energies (RSE) in CubN and DobN. This can be done *via* the known correlation between the Lagrangian kinetic energy density $G(r)$ and RSE.[47] The $G(r)$ values can be easily obtained from the electron density and its Laplacian using the Abramov gradient expansion.[48] Taking into account that RSE and $G(r)$ are directly proportional, the DobN allotrope has a more strained cycle as compared to CubN (Table 3). Although the comparison of the absolute values of $G(r)$ for different types of rings can lead to a significant error, qualitative analysis can be done. Thus, we can conclude that the three-membered nitrogen cycles in CubN and DobN are a few times more strained as compared to aziridine ($G(r)$ = 0.1755 a.u.).[47]

Finally, we calculated the aromaticity of the nitrogen rings in CubN and DobN using the known magnetic criterion NICS (nucleus-independent chemical shift).[49] For this purpose, we have applied hydrogen-terminated model structures that retain at least two N–N bonds between the ring and the hydrogen atoms (Fig. S2 in the ESI†). As follows from the calculated NICS values (Table 4), the three-membered nitrogen cycles are aromatic. Moreover, the CubN allotrope is more stabilized by aromaticity than DobN. The main contribution in stabilization comes from σ-aromaticity (NICS(0)); however, classical π-aromaticity is also important and is comparable with that of benzene.[49]

To ensure that the studied allotropes can be accessible at ambient pressure, we analyzed their dynamical and mechanical stability. The calculations of phonon dispersion at zero pressure revealed the dynamical stability of the studied allotropes (Fig. 2). As follows from Fig. 2, the DobN allotrope has several modes above 1400 cm^{-1}. These are the N(1)=N(4) bond vibrations (Fig. 1e), which will be discussed below in more detail. Both phonon spectra demonstrate the linearity of the three acoustic branches near the Γ-point as well as a complete absence of the soft modes. The latter spectral feature also remains unchanged at high pressures; thus, we can conclude that the

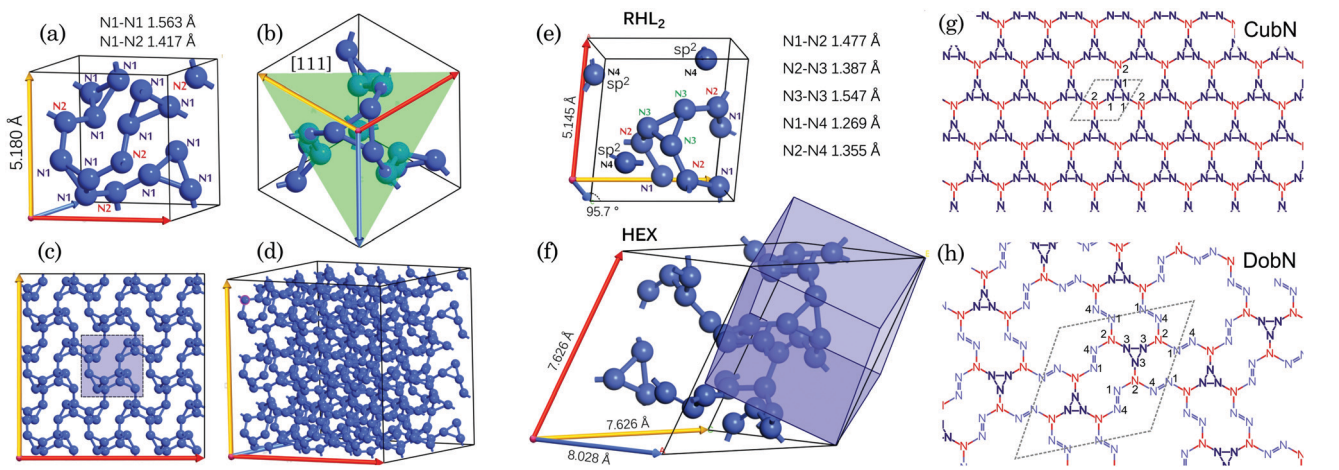

Fig. 1 Projections of the unit cell of CubN (a and b) and the corresponding crystal packing (c and d); the asymmetric cell of DobN in the RHL_2 (e) and HEX (f) lattices; the corresponding 2D topology (g and h). The symmetry-unique bond lengths are also presented.

Table 4 The calculated NICS values for the CubN and DobN allotropes

Allotrope	NICS(0)	NICS(0.5)	NICS(1.0)
CubN	−25.7	−11.0	−3.3
DobN	−20.1	−6.4	−0.3

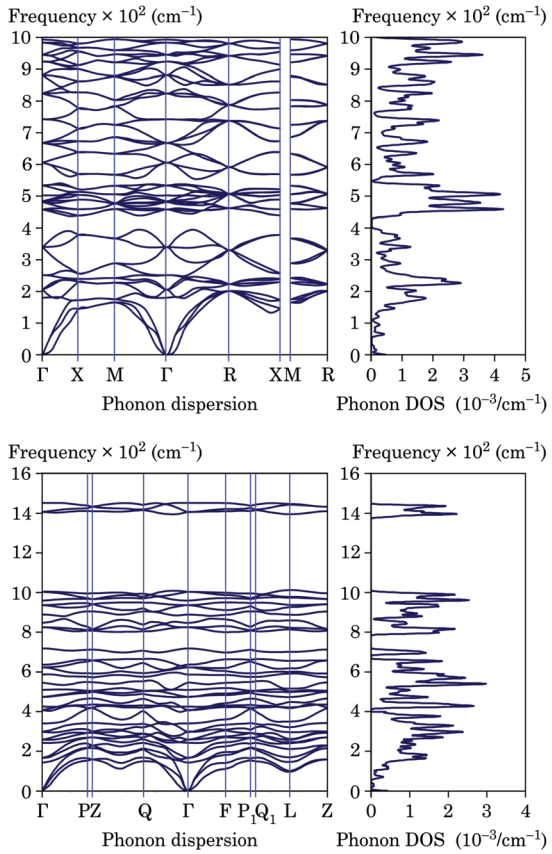

Fig. 2 Zero-pressure phonon dispersion and density of phonon states of the CubN (top) and DobN (bottom) allotropes.

studied nitrogen allotropes are dynamically stable and can exist at ambient pressure.

The corresponding mechanical stability was studied using the Born–Huang criteria. For the Laue classes $m\bar{3}$ and $\bar{3}$ these criteria are as follows:[50]

$$C_{11} - C_{12} > 0;\ C_{11} + 2C_{12} > 0;\ C_{44} > 0 \quad (1)$$

$$\begin{cases} C_{11} > |C_{12}|;\ C_{44} > 0; \\ C_{13}^2 < 1/2C_{33}(C_{11} + C_{12}); \\ C_{14}^2 + C_{15}^2 < 1/2C_{44}(C_{11} - C_{12}) \equiv C_{44}C_{66}. \end{cases} \quad (2)$$

The independent elastic stiffness constants (C_{ij}), which are calculated using the energy-*vs.*-strain method, are listed in Table 5. Along with the C_{ij} values, Young's modulus (E), bulk (B) moduli and Poisson's ratio (ν) are included. As one can see in Table 5, the CubN and DobN allotropes demonstrate mechanical stability. These materials are much softer as compared to cg-N

Table 5 The calculated mechanical properties of the CubN and DobN (the RHL_2 lattice) allotropes

Phase	E	ν	B	C_{11}	C_{12}	C_{44}
cg-N	459.0	0.1858	243.5	501.6	114.5	238.1
TrigN	249.2[a]	0.3014[b]	173.9	291.8[c]	82.7	264.1
CubN	116.1	0.2024	65.0	129.3	32.8	44.4
DobN	34.4[d]	0.2150[e]	32.9	48.2[f]	19.0	13.7

[a] This value is $E_x \equiv E_y$, while E_z = 747.7 GPa. [b] This value is $\nu_{xy} \equiv \nu_{yx}$, while $\nu_{zx} \equiv \nu_{zy}$ = 0.2233 and $\nu_{xz} \equiv \nu_{yz}$ = 0.0744. [c] The rest independent constants are C_{13} = 83.6 GPa, C_{14} = 45.0 GPa, C_{15} = −17.4 GPa and C_{33} = 785.0 GPa. [d] This value is $E_x \equiv E_y$, while E_z = 44.1 GPa. [e] This value is $\nu_{xy} \equiv \nu_{yx}$, while $\nu_{zx} \equiv \nu_{zy}$ = 0.4181 and $\nu_{xz} \equiv \nu_{yz}$ = 0.2150. [f] The rest independent constants are C_{13} = 28.1 GPa, C_{14} = 0.5 GPa, C_{15} = 2.5 GPa and C_{33} = 67.6 GPa.

and TrigN and occupy an intermediate position between the typical covalent and molecular crystals.

As seen in Fig. 3, the mechanical strength distribution is rather uniform in space and for DobN, the maximum changes do not exceed about 10 GPa. It is interesting that the Poisson's ratios ($\nu_{zx} \equiv \nu_{zy}$) for DobN are very high and are about twice as high as the other values (Table 5).

Since the Earth's pressures reflect only a tiny part of the Universe's conditions, we have calculated the CubN and DobN allotropes at increased pressures; the results are presented graphically in Fig. 4. Herein, we have compared the energies of various nitrogen phases with α-N_2 as the most stable low-temperature, low-pressure phase. For a more correct comparison, however, two additional molecular phases of nitrogen, which are stable at higher pressures, namely, ε-N_2 and ζ-N_2, were included.[51] As can be seen in Fig. 4a, CubN and DobN became more stable than α-N_2 at about 90 and 130 GPa. Moreover, at 200 GPa, CubN becomes lower in energy than all molecular nitrogen phases considered. The DobN allotrope, however, remained a relatively high-lying phase in the entire pressure range.

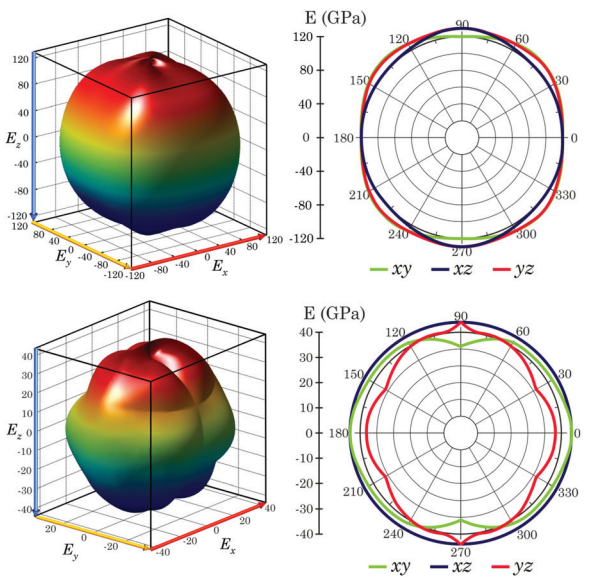

Fig. 3 Graphical 3D representation of the Young's modulus and its projections on three secant planes for CubN (top) and DobN (bottom).

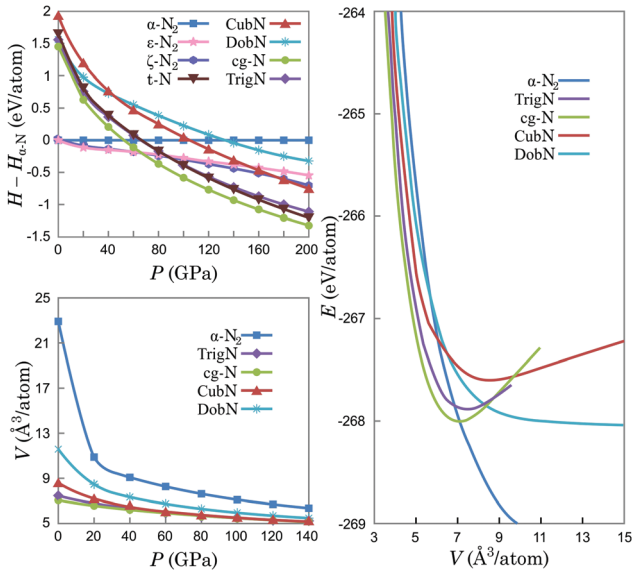

Fig. 4 Pressure-dependence of the relative enthalpies (a) and volume (b); the equation of state $E(V)$.

Electronic and spectral properties

Since the band gap value is very sensitive to the methods applied, we have used our previous approach NCP/HSE06/700 eV.[17] This approximation was carefully calibrated in order to obtain stable reproducible results depending on the k-mesh tightness and the energy cutoff. It is known that the hybrid functional HSE06 provides good band gaps, which are usually approximately 1–1.5 eV higher than those obtained with pure functionals.[52,53] In this work, we have used the standardized approach for the Brillouin zone (BZ) integration (the so-called high-throughput band structure calculations).[54] The corresponding BZ paths are illustrated in Fig. S3 in the ESI.† The calculated band structure plots of the CubN and DobN allotropes are illustrated in Fig. 5. As can be seen in the plot, both materials demonstrate indirect band gaps of 4.090 eV and 2.694 eV, respectively. Valence band maximum (VBM) and conduction band minimum (CBM) for CubN correspond to the $X \rightarrow \Gamma$ transition and for DobN this is $\Gamma \rightarrow P$.

Apart from the band structure, we have calculated the optical properties of the CubN and DobN allotropes. The corresponding absorption spectra are presented in Fig. 6 and the other optical properties (reflectivity, refractive index, dielectric function, conductivity and loss function) are presented in Fig. S4 in the ESI.† Both allotropes absorb in the UV region and are expected to be transparent solids. To better understand the nature of the electronic transitions in the absorption spectra, we performed TD DFT calculations. The first twelve electron excitations are described in Table 6 and the nature of the electronic bands that are involved in the transitions are presented in Fig. S5 in the ESI.† The first maximum in the absorption spectrum of CubN lies at 285 nm and corresponds to the first three degenerate singlet excitations S_1–S_3 (Table 6). In the case of DobN, the first absorption peak is located at 400 nm; it corresponds to the first two degenerate transitions (S_1 and S_2). However, this

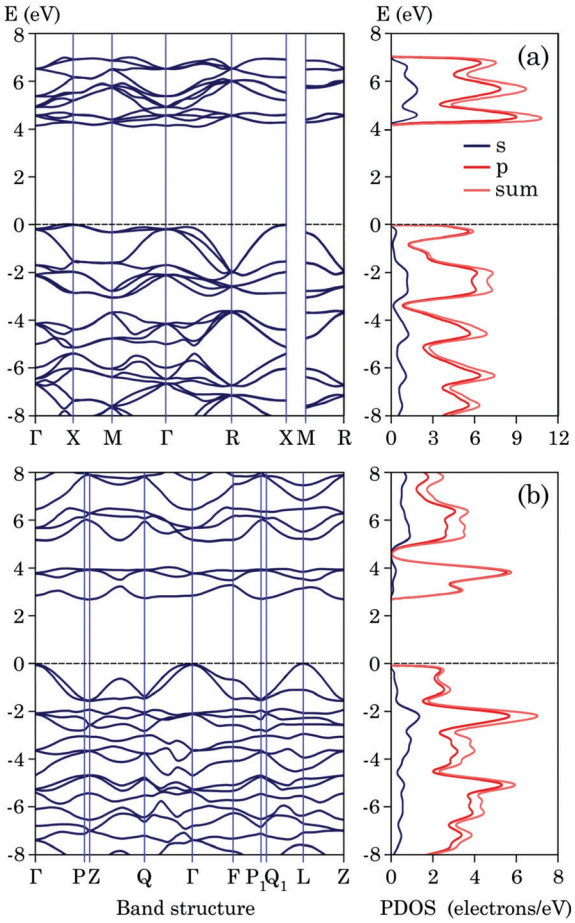

Fig. 5 Band structure and partial density of states (PDOS) for the CubN (top) and DobN (bottom) allotropes calculated using the NCP/HSE06/700 eV approach.

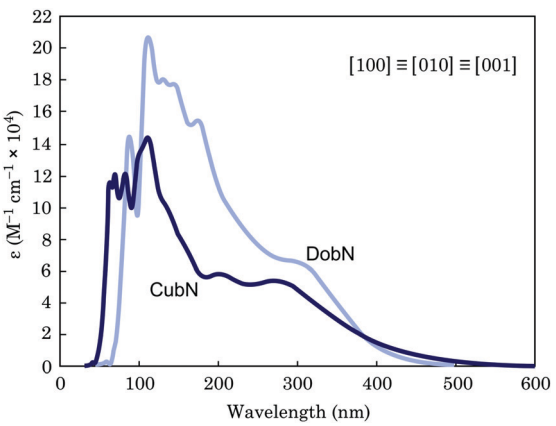

Fig. 6 The calculated absorption spectra of the studied allotropes.

absorption band is masked by a much more intense peak at 329 nm (the S_3 transition).

Another important spectral characterization includes vibrational spectroscopy. In this work, we have calculated infrared (IR) and Raman spectra; the latter are illustrated in Fig. 7. The IR spectra of CubN, DobN, TrigN and cg-N are presented in

Table 6 Energies (eV) and band assignments of the electron transitions in the absorption spectra of CubN and DobN

	CubN		DobN	
State	E (eV)	Assignment	E (eV)	Assignment
S_1	4.352	VB − 1 → CB (0.16) VB → CB (0.72)	3.098	VB − 1 → CB (0.42) VB → CB (0.54)
S_2	4.352	VB − 2 → CB (0.87)	3.098	VB − 1 → CB (0.54) VB → CB (0.42)
S_3	4.352	VB − 1 → CB (0.73) VB → CB (0.15)	3.770	VB − 1 → CB + 1 (0.49) VB → CB + 2 (0.49)
S_4	4.574	VB − 1 → CB + 1 (0.11) VB − 1 → CB + 3 (0.32) VB → CB + 1 (0.12) VB → CB + 2 (0.35)	3.992	VB − 1 → CB + 1 (0.31) VB − 1 → CB + 2 (0.15) VB → CB + 1 (0.15) VB → CB + 2 (0.31)
S_5	4.574	VB − 2 → CB + 1 (0.22) VB − 2 → CB + 2 (0.25) VB − 2 → CB + 3 (0.11) VB − 1 → CB + 1 (0.21) VB → CB + 3 (0.18)	3.992	VB − 1 → CB + 1 (0.15) VB − 1 → CB + 2 (0.31) VB → CB + 1 (0.31) VB → CB + 2 (0.15)
S_6	4.636	VB − 2 → CB + 1 (0.11) VB − 2 → CB + 3 (0.25) VB − 1 → CB + 3 (0.13) VB → CB + 1 (0.32)	3.992	VB − 1 → CB + 2 (0.48) VB → CB + 1 (0.48)
S_7	4.636	VB − 2 → CB + 2 (0.33) VB − 1 → CB + 1 (0.37)	4.665	VB − 2 → CB (0.95)
S_8	4.636	VB − 2 → CB + 2 (0.14) VB − 1 → CB + 3 (0.22) VB → CB + 2 (0.21) VB → CB + 3 (0.19)	4.835	VB − 4 → CB (0.91)
S_9	4.663	VB − 2 → CB + 1 (0.19) VB − 2 → CB + 3 (0.10) VB − 1 → CB + 2 (0.21) VB → CB + 3 (0.15)	4.835	VB − 3 → CB (0.91)
S_{10}	4.799	VB − 2 → CB + 1 (0.30) VB − 2 → CB + 2 (0.13) VB − 1 → CB + 1 (0.13) VB − 1 → CB + 3 (0.14)	5.178	VB − 1 → CB + 3 (0.65) VB → CB + 3 (0.22)
S_{11}	4.799	VB − 1 → CB + 2 (0.46) VB → CB + 1 (0.10) VB → CB + 3 (0.18)	5.178	VB − 1 → CB + 3 (0.22) VB → CB + 3 (0.65)
S_{12}	4.799	VB − 2 → CB + 3 (0.32) VB → CB + 1 (0.21) VB → CB + 2 (0.11)	5.417	VB − 1 → CB + 4 (0.33) VB − 1 → CB + 5 (0.13) VB → CB + 4 (0.13) VB → CB + 5 (0.33)

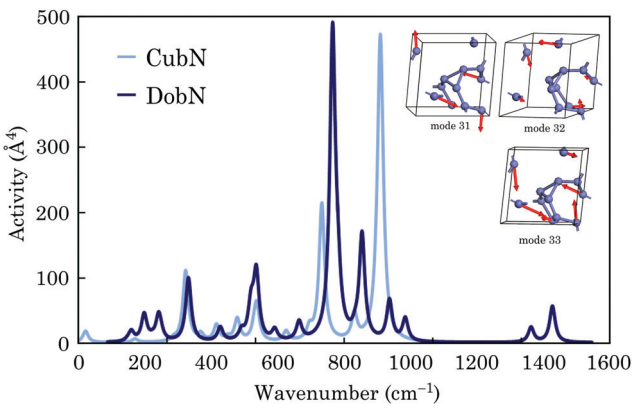

Fig. 7 The calculated Raman spectra of CubN and DobN. Inset: Eigenvectors of the N═N valence bonds vibrations in DobN.

Fig. S6 (ESI†), while the numerical spectral data and forms of vibrations are presented in Table S1 and Fig. S7 in the ESI.† The most active vibration in the Raman spectrum of CubN lies at 910 cm^{-1} and corresponds to the "breathing" of the three-membered cycles (Fig. S7 in the ESI†). In the Raman spectrum of DobN, the most active vibration (at 767 cm^{-1}) has the same nature. The two vibrational peaks around 1400 cm^{-1} are the valence vibrations of the N1═N4 double nitrogen bonds in the DobN allotrope. These are the vibrational modes 31–33, which are graphically presented as insets in Fig. 7. We should also stress that we are not familiar with any other stable predicted polymeric phases of nitrogen possessing double bonds.

Finally, we have calculated the nuclear magnetic resonance (NMR) properties of the studied nitrogen allotropes; the numerical results are gathered in Table S2 in the ESI.†

Thermodynamics, detonation and propulsive properties

It is known that single-bonded nitrogen allotropes bear a huge excess of internal energy and, if synthesized, these can be raw material for the production of highly energetic "green" explosives. Thus, we have estimated the thermodynamic properties of CubN and DobN in order to calculate their detonation and ballistic performances. The temperature dependence of the

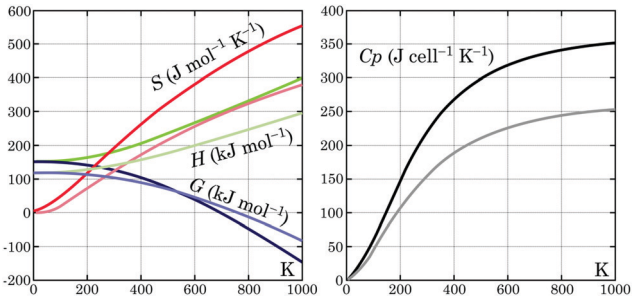

Fig. 8 Temperature dependence of the calculated thermodynamic functions of CubN (deep colors) and DobN (pale colors).

Table 7 The calculated heats of formation (kJ mol^{-1} atom^{-1}) for several nitrogen allotropes at the different levels of theory

Allotrope	HSE06	B3LYP	PBE0	PBE	CA-PZ
cg-N	162.16	185.11	150.14	141.97	84.09
TrigN	172.18	180.71	161.04	152.78	96.87
CubN	212.20	212.82	198.18	181.43	136.34
DobN	170.13	172.01	158.38	143.03	103.15

main thermodynamic functions of these materials is presented graphically in Fig. 8 and the numerical values at 298 K are listed in Table S3 in the ESI.† Additionally, we calculated heats of formation (HOF) for the studied allotropes using different functionals. These values correspond to simple energy differences between the given phase and molecular nitrogen as the most stable one.

The numerical data on heats of formation are presented in Table 7, where it can be seen that all the hybrid functionals provide higher HOFs than pure GGA and LDA. In this paper, we have used the values obtained with the HSE06 functional; however, the predictive force of different functionals is the matter of a separate study. Thus, having the HOF values and crystal densities (Table 8) we have applied the Kamlet–Jacobs empirical scheme[55] to calculate the detonation properties of CubN and DobN. For any nitrogen allotrope, the appropriate structural criterion is as follows: $d \geq 2a + b/2$, where a, b, and d stand for the number of carbon, hydrogen, and oxygen atoms in the asymmetric cell, respectively. Herein, the N, $\bar{M}$ and Q values are expressed in eqn (3) and (4).[55]

$$N = \frac{1}{\bar{M}} = \frac{2c}{4\mathrm{MW}} \quad (3)$$

$$Q = \frac{239\Delta H_f^0}{\mathrm{MW}}, \quad (4)$$

Table 8 Detonation properties for several single-bonded allotropes of nitrogen

Allotrope	ρ (g cm^{-1})	Q (cal g^{-1})	D (km s^{-1})	P (GPa)
cg-N	3.29	2766.89	16.80	167.60
TrigN	3.11	2937.86	16.30	154.32
CubN	2.69	3620.73	15.31	128.17
DobN	2.07	2902.96	11.89	67.96

Table 9 The calculated propulsive properties for several nitrogen allotropes as monopropellants

Allotrope	CCT (K)	I_{sp} (s)	I_{vac} (s)	c^* (m s^{-1})
cg-N	6922	478	491	2679
TrigN	7005	456	500	2728
CubN	7330	488	535	2921
DobN	6988	454	498	2718

where c is the number of nitrogen atoms per asymmetric cell and MW is the molecular weight. The obtained results are listed in Table 8, where CubN and DobN demonstrate lower detonation pressure and velocity compared to TrigN and cg-N, but these values are still much higher than that of conventional explosives based on C–H–N–O or similar formulations.

Additionally, we have estimated the properties of single-bonded nitrogen allotropes as solid propellants. For this purpose we have applied the NASA CEA2 program.[56] Using our previously described code i97creator[57] and the PAC99 routine, we have converted CASTEP thermodynamic properties (Fig. 8) into the form of NASA 9 coefficients.[58] These entries are included in the ESI.†

The predicted properties of four single-bonded nitrogen allotropes as solid monopropellants are listed in Table 9. These materials demonstrate excellent propulsion performance, including very high specific impulse (I_{sp}), vacuum specific impulse (I_{vac}) and characteristic velocity (c^*). The huge energy release caused upon phase transition generates a very high combustion chamber temperature (CCT), near 7000 K for all the allotropes. This process can be expressed as the following:

$$\mathrm{N_{(cr)}} \rightarrow a\mathrm{N_{(g)}} + b\mathrm{N_{2(g)}}.$$

The coefficients a and b for various exit-to-throat area ratios (A_e/A_t) are presented in Table S4 in the ESI.† In the combustion chamber, the coefficient a always exceeds b, but with the rise in A_e/A_t, the relative amount of molecular nitrogen dramatically rises.

Conclusions

We have presented two single- and double-bonded nitrogen allotropes (DobN and CubN), which are built from the three-membered nitrogen cycles. Due to the latter structural motifs, these allotropes have more energy enclosed as compared to the cg-N phase, which is the most stable polymeric phase at high pressures. On the other hand, our calculations suggest the dynamical and mechanical stability of CubN and DobN even at ambient pressure. Thus, these allotropes deserve careful further study using diamond anvil cell experiments or other techniques to provide experimental evidence of their existence.

Herein, we have compared a number of physical properties of DobN and CubN with two other similar allotropes (cg-N and TrigN). The focus was on their detonation and propulsive properties. In this work, we have applied the Kamlet-Jacobs empirical scheme to obtain detonation energies, pressures and velocities. Also, we have developed a procedure to calculate the propulsive characteristics of such allotropes, including specific impulses and characteristic velocities. The results revealed the

huge potential of nitrogen allotropes as high-energy-density materials (HEDM) and, if synthesized, these can be very attractive green energetic materials.

Some theoretical aspects of the thermal stability still remain unclear. Thus, metadynamics simulations are desirable to determine the range of thermal stability of CubN and DobN. This will be the issue of further studies.

Conflicts of interest

There are no conflicts to declare.

Acknowledgements

This work was supported by the Ministry of Education and Science of Ukraine, Research Fund (Grant No. 0118U003862).

Notes and references

1 M. Falcone, L. Chatelain, R. Scopelliti, I. Živković and M. Mazzanti, *Nature*, 2017, **547**, 332–335.
2 M.-A. Légaré, M. Rang, G. Bélanger-Chabot, J. I. Schweizer, I. Krummenacher, R. Bertermann, M. Arrowsmith, M. C. Holthausen and H. Braunschweig, *Science*, 2019, **363**, 1329–1332.
3 I. Valov, B. Luerssen, E. Mutoro, L. Gregoratti, R. A. De Souza, T. Bredow, S. Günther, A. Barinov, P. Dudin, M. Martind and J. Janek, *Phys. Chem. Chem. Phys.*, 2011, **13**, 3394–3410.
4 J. M. P. Martirez and E. A. Carter, *Sci. Adv.*, 2017, **3**, eaao4710.
5 A. V. Pelevkin and A. S. Sharipov, *J. Phys. D: Appl. Phys.*, 2018, **51**, 184003.
6 M. P. Shaver and M. D. Fryzuk, *Adv. Synth. Catal.*, 2003, **345**, 1061–1076.
7 M. I. Eremets, A. G. Gavriliuk, I. A. Trojan, D. A. Dzivenko and R. Boehler, *Nat. Mater.*, 2004, **3**, 558–563.
8 A. K. McMahan and R. LeSar, *Phys. Rev. Lett.*, 1985, **54**, 1929–1932.
9 C. Mailhiot, L. H. Yang and A. K. McMahan, *Phys. Rev. B: Condens. Matter Mater. Phys.*, 1992, **46**, 14419–14435.
10 D. Tomasino, M. Kim, J. Smith and C.-S. Yoo, *Phys. Rev. Lett.*, 2014, **113**, 205502.
11 Y. Ma, A. R. Oganov, Z. Li, Y. Xie and J. Kotakoski, *Phys. Rev. Lett.*, 2009, **102**, 065501.
12 S. Duwal, Y.-J. Ryu, M. Kim, C.-S. Yoo, S. Bang, K. Kim and N. Hwi Hur, *J. Chem. Phys.*, 2018, **148**, 134310.
13 Z. Wu, E. M. Benchafia, Z. Iqbal and X. Wang, *Angew. Chem., Int. Ed.*, 2014, **126**, 12763–12767.
14 B. Hirshberg, R. B. Gerber and A. I. Krylov, *Nat. Chem.*, 2014, **6**, 52–56.
15 M. J. Greschner, M. Zhang, A. Majumdar, H. Liu, F. Peng, J. S. Tse and Y. Yao, *J. Phys. Chem. A*, 2016, **120**, 2920–2925.
16 Y. Li, X. Feng, H. Liu, J. Hao, S. A. T. Redfern, W. Lei, D. Liu and Y. Ma, *Nat. Commun.*, 2018, **9**, 722.
17 S. V. Bondarchuk and B. F. Minaev, *Phys. Chem. Chem. Phys.*, 2017, **19**, 6698–6706.
18 S. V. Bondarchuk and B. F. Minaev, *Comput. Mater. Sci.*, 2017, **133**, 122–129.
19 D. K. Spaulding, G. Weck, P. Loubeyre, F. Datchi, P. Dumas and M. Hanfland, *Nat. Commun.*, 2014, **5**, 5739.
20 M. I. Eremets, I. A. Trojan, A. G. Gavriliuk and S. A. Medvedev, Synthesis of High-Nitrogen Energetic Material, in *Static Compression of Energetic Materials*, eds. S. M. Peiris, G. J. Piermarini, Springer-Verlag, Berlin, Heidelberg, 2008, pp. 75–97.
21 T. M. Klapötke, New Nitrogen-Rich High Explosives, in *High Energy Density Materials*, ed. T. M. Klapötke, Springer-Verlag, Berlin, Heidelberg, 2007, pp. 85–121.
22 J. S. Lin, A. Qteish, M. C. Payne and V. Heine, *Phys. Rev. B: Condens. Matter Mater. Phys.*, 1993, **47**, 4174–4180.
23 J. P. Perdew, K. Burke and M. Ernzerhof, *Phys. Rev. Lett.*, 1996, **77**, 3865–3868.
24 G. Kresse and D. Joubert, *Phys. Rev. B: Condens. Matter Mater. Phys.*, 1999, **59**, 1758–1775.
25 D. M. Ceperley and B. J. Alder, *Phys. Rev. Lett.*, 1980, **45**, 566–569.
26 A. D. Becke, *J. Chem. Phys.*, 1993, **98**, 5648–5652.
27 C. Adamo and V. Barone, *J. Chem. Phys.*, 1998, **110**, 6158–6170.
28 J. Heyd and G. Scuseria, *J. Chem. Phys.*, 2004, **121**, 1187–1192.
29 S. Grimme, *J. Comput. Chem.*, 2006, **27**, 1787–1799.
30 G. Kresse and J. Furthmüller, *Phys. Rev. B: Condens. Matter Mater. Phys.*, 1996, **54**, 11169–11186.
31 F. Ortmann, F. Bechstedt and W. G. Schmidt, *Phys. Rev. B: Condens. Matter Mater. Phys.*, 2006, **73**, 205101.
32 M. C. Payne, M. P. Teter, D. C. Allan, T. A. Arias and J. D. Joannopoulos, *Rev. Mod. Phys.*, 1992, **64**, 1045–1097.
33 R. Fletcher, *Practical Methods of Optimization*, Wiley, New York, 1980.
34 S. Hirata and M. Head-Gordon, *Chem. Phys. Lett.*, 1999, **314**, 291–299.
35 S. J. Clark, M. D. Segall, C. J. Pickard, P. J. Hasnip, M. J. Probert, K. Refson and M. C. Payne, *Z. Kristallogr. - Cryst. Mater.*, 2005, **220**, 567–570.
36 Materials Studio 7.0, Accelrys, Inc., San Diego, CA, 2013.
37 P. Giannozzi, S. Baroni, N. Bonini, M. Calandra, R. Car, C. Cavazzoni, D. Ceresoli, G. L. Chiarotti, M. Cococcioni, I. Dabo, A. Dal Corso, S. Fabris, G. Fratesi, S. de Gironcoli, R. Gebauer, U. Gerstmann, C. Gougoussis, A. Kokalj, M. Lazzeri, L. Martin-Samos, N. Marzari, F. Mauri, R. Mazzarello, S. Paolini, A. Pasquarello, L. Paulatto, C. Sbraccia, S. Scandolo, G. Sclauzero, A. P. Seitsonen, A. Smogunov, P. Umari and R. M. Wentzcovitch, *J. Phys.: Condens. Matter*, 2009, **21**, 395502.
38 Virtual NanoLab 2016.3, QuantumWise A/S, www.quantumwise.com.
39 A. Otero-De-La-Roza, E. R. Johnson and V. Luaña, *Comput. Phys. Commun.*, 2014, **185**, 1007–1018.
40 W. Tang, E. Sanville and G. Henkelman, *J. Phys.: Condens. Matter*, 2009, **21**, 084204.
41 Ch. Leuenberger, L. Hoesch and A. S. Dreiding, *J. Chem. Soc., Chem. Commun.*, 1980, 1197–1198.
42 M. T. Nguyen, J. Kaneti, L. Hoesch and A. S. Dreiding, *Helv. Chim. Acta*, 1984, **67**, 1918–1929.

43 R. Peverati, J. S. Siegel and K. K. Baldridge, *Phys. Chem. Chem. Phys.*, 2009, **11**, 2387–2395.

44 A. Karahodza, K. J. Knaus and D. W. Ball, *THEOCHEM*, 2005, **732**, 47–53.

45 W. Chi, B. Li and H. Wu, *Struct. Chem.*, 2013, **24**, 375–381.

46 A. G. Orpen, L. Brammer, L. H. Allen, O. Kennard, D. G. Watson and R. Taylor, Typical interatomic distances: organometallic compounds and coordination complexes of the d- and f-block metals. in *International Tables for Crystallography*, ed. H.-B. Bürgi and J. D. Dunitz, Wiley, New York, 2006, pp. 751–858.

47 A. Bauzá, D. Quiñonero, P. M. Deyà and A. Frontera, *Chem. Phys. Lett.*, 2012, **536**, 165–169.

48 Yu. A. Abramov, *Acta Crystallogr., Sect. A: Found. Crystallogr.*, 1997, **53**, 264–272.

49 Z. Chen, C. S. Wannere, C. Corminboeuf, R. Puchta and P. v. R. Schleyer, *Chem. Rev.*, 2005, **105**, 3842–3888.

50 F. Mouhat and F.-X. Coudert, *Phys. Rev. B: Condens. Matter Mater. Phys.*, 2014, **90**, 224104.

51 E. Gregoryanz, A. F. Goncharov, R. J. Hemley, H.-K. Mao, M. Somayazulu and G. Shen, *Phys. Rev. B: Condens. Matter Mater. Phys.*, 2002, **66**, 224108.

52 S. V. Bondarchuk and B. F. Minaev, *New J. Chem.*, 2017, **41**, 13140–13148.

53 S. V. Bondarchuk, *New J. Chem.*, 2019, **43**, 1459–1468.

54 W. Setyawan and S. Curtarolo, *Comput. Mater. Sci.*, 2010, **49**, 299–312.

55 M. J. Kamlet and S. J. Jacobs, *J. Chem. Phys.*, 1968, **48**, 23–35.

56 S. Gordon and B. J. McBride, Computer program for calculation of complex chemical equilibrium compositions and applications. I. Analysis. Cleveland, OH: NASA, 1994 (NASA Reference Publication 1311).

57 S. V. Bondarchuk and N. A. Yefimenko, *Propellants, Explos. Pyrotech.*, 2018, **43**, 818–824.

58 B. J. McBride, M. J. Zehe and S. Gordon, NASA Glenn Coefficients for Calculating Thermodynamic Properties of Individual Species. Cleveland, OH: Glenn Research Center, 2002 (OhioNASA/TP-2002-211556).